



# The Effects of Lithium Ions and pH on the Function of Polyacrylic Acid Binder for Silicon Anodes

Fei Sun<sup>✉</sup> and Dean R. Wheeler<sup>\*,z</sup>

Department of Chemical Engineering, Brigham Young University, Provo, Utah 84602, United States of America

Binder plays a critical role in the performance of silicon anodes for lithium-ion batteries, specifically by connecting particles of active material and promoting adhesion to the current collector. Recent studies have differed on the relative cycle life of silicon anodes made from water-based polyacrylic acid (PAA) vs LiOH-PAA binders. Differences between the two may be due to the pH value or the extra Li<sup>+</sup> in the binder, both of which change when LiOH is added to PAA. Here we investigate the impact of these two variables on the performance of silicon anodes. Regarding the effect of Li<sup>+</sup>, cyclic voltammetry (CV) and electrochemical impedance spectroscopy (EIS) results confirm our hypothesis that the extra Li<sup>+</sup> facilitates ion transport. Regarding pH, we find that high pH in binders is detrimental to the electrode mechanical integrity, as observed in peeling tests and cross-sectional imaging. However, viscosity tests reveal that increased pH benefits the coating and mixing process. Our cycling results show that LiOH-PAA binder maintains greater cell capacity than does PAA, and further that LiOH-PAA at pH 4.5 leads to a cell with the highest capacity. Therefore, an intermediate pH is an optimal compromise between benefits observed for the low and high pH experiments. © 2023 The Electrochemical Society ("ECS"). Published on behalf of ECS by IOP Publishing Limited. [DOI: [10.1149/1945-7111/aceab1](https://doi.org/10.1149/1945-7111/aceab1)]

Manuscript submitted April 20, 2023; revised manuscript received June 23, 2023. Published August 9, 2023.

Graphite is the most commonly used anode active material in lithium-ion batteries because it is abundant, electrically conducting, and can intercalate lithium ions to store electrical charge with a modest volume expansion. However, graphite's low theoretical capacity (372 mAh g<sup>-1</sup>) restricts the maximum capacity of the battery. On the other hand, silicon has emerged as a promising alternative anode material because of its high theoretical capacity (3580 mAh g<sup>-1</sup>), low lithiation/delithiation voltage (<0.5 V vs Li/Li<sup>+</sup>), and potential low cost.<sup>1-3</sup>

Although silicon shows excellent capacity performance, its cycling stability has been limited because of a huge volume change upon lithiation/delithiation. This volume change, which can be as high as 400%, leads to progressive failure modes such as particle pulverization, electrode delamination, and unstable solid electrolyte interphase (SEI) layers, all resulting in a high degree of irreversible capacity loss.<sup>4-6</sup> Moreover, the semiconductor nature of Si makes it challenging to use as an electrode material due to low electronic conductivity.<sup>7</sup>

Hence, a matrix that can effectively buffer the volume expansion would better enable commercial application of silicon electrodes. Binders play a critical role by promoting even dispersion and cohesion of particles, and adhesion to the current collector. A common binder for graphite anodes, polyvinylidene fluoride (PVDF), is not suitable for silicon cells due to weak van der Waals interactions with Si and difficulty accommodating the large silicon volume change.<sup>8</sup> Carboxy-group rich polymers such as polyacrylic acid (PAA) and carboxymethyl cellulose (CMC) exhibit promising characteristics as binders for Si-based anodes. Polar hydrogen bonds form between the carboxy groups of the binder and the Si surface, and furthermore may exhibit a self-healing effect if locally broken.<sup>9,10</sup> PAA-based binders are also competitive in their low cost and easy synthesis.<sup>11</sup>

The use of LiOH to neutralize PAA binder is a widely adopted method for fabricating silicon anode. In the work by Hu et al., adding lithium hydroxide was found to improve the coating process by increasing viscosity at low shear rates and thereby promoting shear-thinning behavior.<sup>12</sup> On the other hand, there have been divergent results regarding the electrochemical performance of cells composed of these two binders. While Hu et al. claimed PAA binder-composed cell has a 59% higher capacity than that of LiOH-PAA,<sup>12</sup> Dang et al. demonstrated a 1000 mAh g<sup>-1</sup> higher capacity of electrodes containing LiOH-PAA binder.<sup>13</sup> Moreover, in the case where lithiated binder-composed cell has a higher

electrochemical performance, it is not yet fully understood why the introducing of lithium hydroxide makes this change. To address this gap and develop a deeper understanding of what makes lithiated PAA binder different than pristine PAA, we separate the two main factors, the pH and the presence of extra Li<sup>+</sup>, to determine how each factor contributes to cell performance.

Initially, we studied the impact of extra Li<sup>+</sup> by performing two impedance tests on multiple binder films. The results indicate that the LiOH-PAA binder has a higher ionic conductivity. Furthermore, we conducted viscosity tests, peeling tests, and cross-sectional scanning electron microscopy (SEM) imaging to investigate the effect of pH. Our findings suggest that for our series of binder formulations, binder pH 4.5 produces superior cell performance to that of pH 2 or pH 7. Finally, cycling results of different binder-composed cells are compared to confirm the prior experiments.

## Experimental

**Materials and equipment.**—Carbon black (C45) was obtained from Timcal. Silicon nanoparticles (~100 nm) were purchased from Nanostructured & Amorphous Materials, Inc. Polyacrylic acid (PAA, MW = 450 kDa), lithium hydroxide, and ammonium hydroxide were acquired from Sigma-Aldrich. Annealed copper sheets were purchased from Nimrod Copper Co. Electrolyte (1.0 M LiPF<sub>6</sub> in EC and DEC with a volume ratio of 50:50) and fluoroethylene carbonate (FEC) were purchased from Sigma-Aldrich. Electrochemical tests were conducted using a Maccor 4300 battery tester.

**Binder preparation.**—The neutralization procedure was achieved by adding different amounts of bases into PAA solutions. The PAA solution was prepared by mixing PAA powder with deionized water with a weight ratio of 1:12 at 22 °C for 6 h. The container was covered with a lid to minimize water evaporation. A base (e.g. LiOH) was then added into the PAA solution and mixed for another 3 h until desired pH was achieved. pH values were measured with one or more pH strips, depending on the appropriate pH range (MQuant, ranges 0–14, 2.5–4.5 and 4–7) that was contacted with the binder solution. The same procedure was done for the preparation of NH<sub>3</sub>-PAA and NaOH-PAA binder solutions.

The molar ratio of base to PAA monomer controls the resulting binder solution pH as shown in Fig. 1. When the LiOH-PAA solution reaches pH 4.5, this corresponds to a molar ratio of LiOH/PAA of 0.35. This corresponds to a state of partial deprotonation, based on approximately one lithium ion replacing a dissociated proton in the polymer. Note that the pK<sub>a</sub> value for PAA is 4.5.<sup>14</sup>

\*Electrochemical Society Member.

<sup>z</sup>E-mail: [dean\\_wheeler@byu.edu](mailto:dean_wheeler@byu.edu)

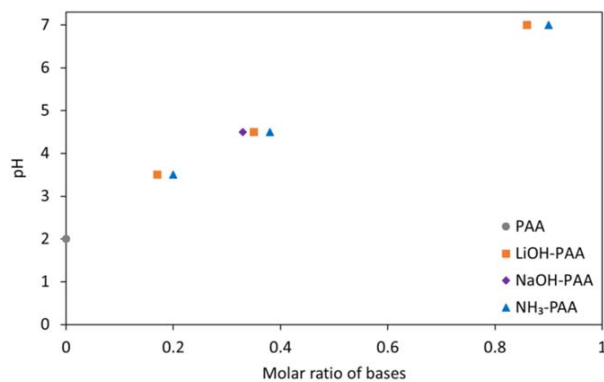


**Figure 1.** Effect of molar ratio of base to PAA monomer on resulting binder solution pH.

**Electrode preparation.**—The fabricated silicon electrodes were composed of 60 wt% silicon, 30 wt% binder, and 10 wt% C45. The binder preparation procedure is given above. Dry silicon and carbon black powders were ground with a mortar and pestle for 20 min. The PAA binder solution and ground particles were then mixed in a sealed jar using a high-speed rotating homogenizer (Algimax GX 300) for 24 s. For the coating process, a 7 cm × 9 cm copper sheet was first cleaned using isopropyl alcohol. The electrode slurry was then coated on the copper sheet using a four-sided coating applicator with a 75 μm thickness side. The anode was subsequently dried in an oven at 66 °C for 6 h and calendered to achieve a 50% porosity.

**Cell assembly and electrochemical characterization.**—Half cells were assembled using a silicon composite electrode as the working electrode, a lithium metal counter electrode, a microporous polypropylene separator (Celgard 2325) and 1.0 M LiPF<sub>6</sub> in EC:DEC:FEC (45:45:10 by volume) electrolyte. All cells were allowed to soak in the electrolyte overnight to ensure thorough penetration of the electrodes. Cycling was performed using a Maccor 4300 battery tester; each cell underwent 3 formation cycles at C/20 rate, followed by 4 cycles each at C/10, C/5, C/3, 1 C and 2 C rates with a voltage window of 0.05 to 1.5 V. The sequence of cycles is then repeated a second time, for a total of 40 cycles. All electrochemical measurements were conducted at 22 °C.

**Impedance tests.**—Both cyclic voltammetry (CV) and electrochemical impedance spectroscopy (EIS) tests were performed using Bio-Logic SP 200 to determine binder impedance. To isolate the effect of binder, no active material or carbon additives were used in these tests. The binder films were prepared by dissolving 3 g of PAA in 18 g of deionized water and stirring the mixture for 6 h. Different pH values were then achieved by adding various amounts of lithium hydroxide, ammonia hydroxide or sodium hydroxide. The binder slurries were then poured into a mold to 1 mm depth and air dried for 24 h, followed by 3 h of oven drying at 77 °C. Each binder film was cut into a 3.7 cm square. For the CV test, a binder film was sandwiched between Celgard layers and then between two lithium

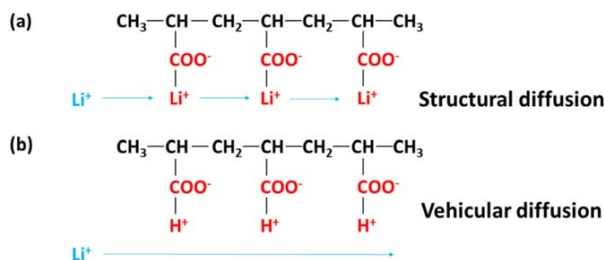


**Figure 2.** Illustration of Li<sup>+</sup> distinct transport mechanisms in PAA binder.

foil electrodes and voltage window is −0.1 V to 0.1 V. For the EIS test, the binder film was sandwiched between Celgard layers and then between two stainless steel sheets. Each cell contained 600 μL of the electrolyte.

**Peeling tests.**—Peeling tests were conducted to evaluate the electrode integrity using an Instron 3343 stress-strain tester to evaluate the adhesion/cohesion of the binders. The laminate side of the electrode, measuring 30 mm × 54 mm, was attached to a strip of 20 mm wide aluminum-backed adhesive tape. The electrode portion underneath the adhesive tape was removed from its current collector by pulling the tape at constant displacement rate of 500 mm min<sup>−1</sup> as described more fully in Ref. 15. The applied force was measured, and load/displacement plots were generated to analyze the results.

**Rheological measurements.**—The shear viscosity was measured for the binder solutions at different shear rates using an AR2000ex rheometer that was equipped with a cone-plate geometry of 20 mm diameter and 2° angle, at a temperature of 22 °C.

**Electrode cross-section analysis.**—All electrodes were milled using a broad ion beam (IB-19530CP JEOL cross-section polisher) at a voltage of 5 kV for 2 h. The cross-sectional microstructure of the electrodes was analyzed using a Thermo Scientific Apreo C scanning electron microscope (SEM).

## Results and Discussion

This section provides the results for the tests on binder performance, namely impedance tests, rheological tests, peeling tests, and cycling tests. In order to examine the effect of Li<sup>+</sup> and pH on PAA, different pH values (2, 3.5, 4.5 and 7) and various cations (H<sup>+</sup>, Li<sup>+</sup>, Na<sup>+</sup>, NH<sub>4</sub><sup>+</sup>) were chosen in this study. For convenience, we designate each binder film or binder-composed electrode using *cation-PAA(pH)*. For instance, NH<sub>3</sub>-PAA(3.5) means the binder is made by addition of aqueous NH<sub>3</sub> to PAA until pH 3.5 is achieved.

**Effect of Li<sup>+</sup> on ionic conductivity.**—Figure 2 illustrates two possible mechanisms for transport, structural and vehicular. Our hypothesis is that the extra Li<sup>+</sup> introduced from LiOH could facilitate Li-ion transport in the binder through a combination of structural and vehicular transport. The structural mechanism of Li-ion transport in LiOH-PAA binder is comparable to the Grotthuss mechanism for proton transport in water.<sup>16</sup> The active Li<sup>+</sup> from one electrode can diffuse through the −COOLi bond network of LiOH-PAA to the counter electrode by forming and breaking associations or bonds between Li<sup>+</sup> and acrylate groups. This type of transport is considered faster than traditional vehicular diffusion because the diffusing species has a shorter distance to move, and the diffusing species does not necessarily carry a shell of solvent molecules with it. In the work by Pieczonka et al., a high-resolution transmission electron microscope (TEM) observation revealed a clear LiOH-PAA film on the outside surface of the active material. Consistent with our above hypothesis, this film was claimed to possess a higher ionic transport ability owing to the presence of intrinsic Li<sup>+</sup>.<sup>17</sup>

To test our hypothesis and directly measure binder ionic conductivity, we conducted cyclic voltammetry (CV) tests and electrochemical impedance spectroscopy (EIS) tests, with the results presented in Fig. 3 and Table 1. Specifically, we compared the ionic conductivity of binder film NH<sub>3</sub>-PAA(4.5) with LiOH-PAA(4.5). Impedance tests conducted on binder film PAA(2) is included for reference. Additionally, binder film conductivities of NaOH-PAA(4.5), NH<sub>3</sub>-PAA(3.5) and NH<sub>3</sub>-PAA(7) are included to examine the cation effect and pH effect. In Fig. 3a, the slope of the CV plot indicates the binder ionic conductivity. Ohm's law ( $\Delta V = IR$ ) and the relationship between resistance  $R$  and conductivity  $k$  for planar samples ( $R = L/kA$ , where  $L$  is thickness and  $A$  is area) allow us to determine the ionic conductivity of each binder film. To summarize,

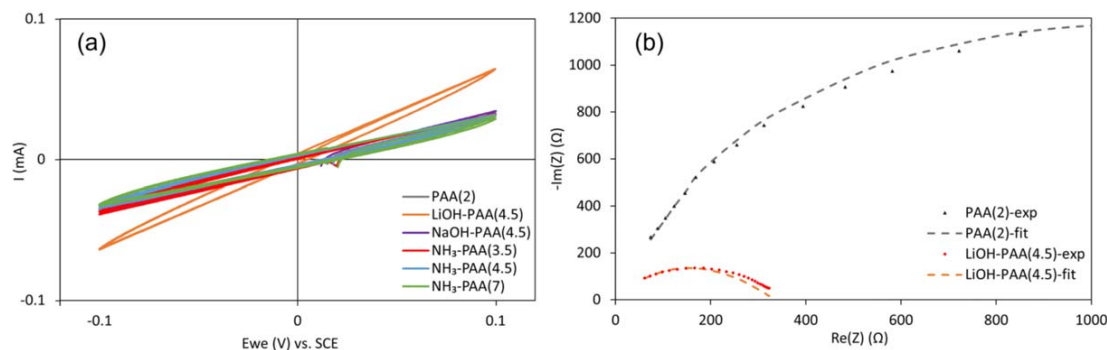


**Figure 3.** (a) CV test of binder films, and (b) EIS test of binder films with experimental data given as points and modeling fits as dashed lines.

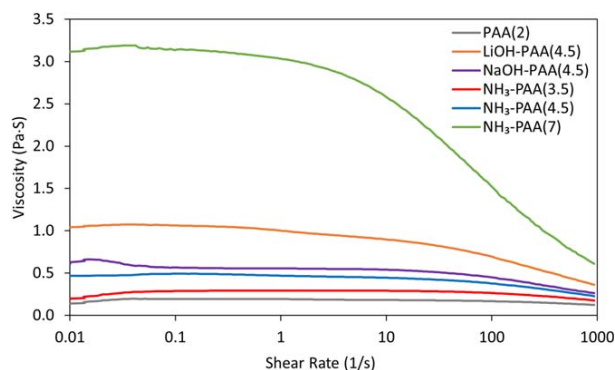


**Figure 4.** Viscosity of PAA, LiOH-PAA and  $\text{NH}_3$ -PAA binder solutions at different shear rates.

the film LiOH-PAA(4.5) has a conductivity twice that of others. In addition,  $\text{NH}_3$ -PAA, NaOH-PAA and pristine PAA exhibit very similar conductivity, around  $0.25 \mu\text{S cm}^{-1}$ . This result indicates that PAA binders based on  $\text{H}^+$ ,  $\text{NH}_4^+$  and  $\text{Na}^+$  cations have very similar conductivities and that all have less conductivity than the LiOH-PAA binder.

Additionally, representative EIS results are included in Fig. 3b. A Randles cell model was used to fit the experimental data. The high-frequency intercept on the real axis determines the ionic resistance of each binder film, which can be converted to conductivity as was done for the CV data, though perhaps there is more uncertainty in the EIS results due to the required extrapolation. For clarity in presentation, the EIS curves for 4 other cases are not given in Fig. 3b, namely NaOH-PAA(4.5) and  $\text{NH}_3$ -PAA(3.5, 4.5, 7). These curves nearly completely overlap with the curve for PAA(2) and their real-axis intercepts on the EIS plot are effectively given by the conductivities in Table I.

Interestingly, all binder films exhibited a qualitative conductivity trend from EIS similar to that observed in the CV test, though the EIS high-frequency conductivities are much higher than for the low-frequency CV test. For example, the LiOH-PAA(4.5) film displays the greatest conductivity compared to the other films, for both sets of experiments. The consistency between the EIS and CV results suggests that the lithiation of the PAA binder can enhance the ionic conductivity and that pH is a lesser effect.

**Effect of pH on particle binding and dispersion.**—The neutralization degree of the binder can potentially affect several parameters that include (1) binder viscosity and subsequent particle sedimentation, (2) particle dispersion, and (3) mechanical integrity of electrodes. Here we report on experiments to evaluate such effects.

**Viscosity and particle sedimentation.**—We investigated the rheological behaviors of binder solutions with different pH values and cations, as is summarized in Fig. 4. Viscosity of pristine PAA(2) is added for reference. The viscosity of NaOH-PAA(4.5), LiOH-PAA(4.5) and  $\text{NH}_3$ -PAA(4.5) binder solutions are included to determine the effect of cation. Compared to pristine PAA, we observed a significant increase in viscosity and shear-thinning effect for these three neutralized binder solutions. For example, the viscosity of pristine PAA(2) binder solution was  $0.2 \text{ Pa-s}$  at  $0.1 \text{ s}^{-1}$  shear rate, while it was 1.1, 0.6, and  $0.5$  for LiOH-PAA(4.5), NaOH-PAA(4.5) and  $\text{NH}_3$ -PAA(4.5), respectively. High viscosity is generally beneficial for the coating process as it improves the stability of the particle suspension by slowing down sedimentation and coalescence. Increased shear-thinning behavior was also observed in all neutralized binder solutions, meaning that viscosity proportionally decreases to a greater degree with increased shear rate. According to the work by Hu et al., the shear-thinning effect facilitates particle dispersion in electrode solution mixing process.<sup>12</sup> Meanwhile, when comparing only the effect of pH on viscosity,  $\text{NH}_3$ -PAA(3.5), (4.5) and (7) binder solutions showed a trend that with the increase of the neutralization degree, the viscosity and shear-thinning behavior are promoted. For instance, at  $1 \text{ s}^{-1}$  shear rate,  $\text{NH}_3$ -PAA(7) has a viscosity 6 and 12 times that of  $\text{NH}_3$ -PAA(4.5) and  $\text{NH}_3$ -PAA(3.5) binder solutions, respectively. According to Dang et al., the substitution of Li in  $-\text{COOH}$  groups can stretch the polyacrylate chains through electrostatic repulsion between neighboring  $-\text{COOLi}$ , which increases viscosity.<sup>13</sup> Shi et al. also reported that the substitution of  $\text{NH}_3 \cdot \text{H}_2\text{O}$  in polyacrylate chains can have a similar effect on the binder solution.<sup>18</sup> These findings are consistent with our experiments.

**Particle dispersion.**—In this study the particles are around  $100 \text{ nm}$  diameter, making them colloidal particles. In a study by Hays et al., it was found that at higher pH values, the zeta potential of nano-Si particles increases in magnitude, leading to a stronger particle-particle repulsion that can overcome the weak van der Waals attractions in the electrode slurry.<sup>19</sup> As a result, the Si particles tend to disperse better, which is beneficial for eventual electrode performance. We did not do any particle dispersion tests with our

**Table I.** Calculated ionic conductivity of binder films from CV and EIS tests.

Binder film	PAA(2)	LiOH-PAA(4.5)	NaOH-PAA(4.5)	$\text{NH}_3$ -PAA(3.5)	$\text{NH}_3$ -PAA(4.5)	$\text{NH}_3$ -PAA(7)
CV ionic conductivity ( $\mu\text{S/cm}$ )	0.24	0.47	0.26	0.26	0.23	0.24
EIS ionic conductivity ( $\mu\text{S/cm}$ )	15	29	15	15	15	15

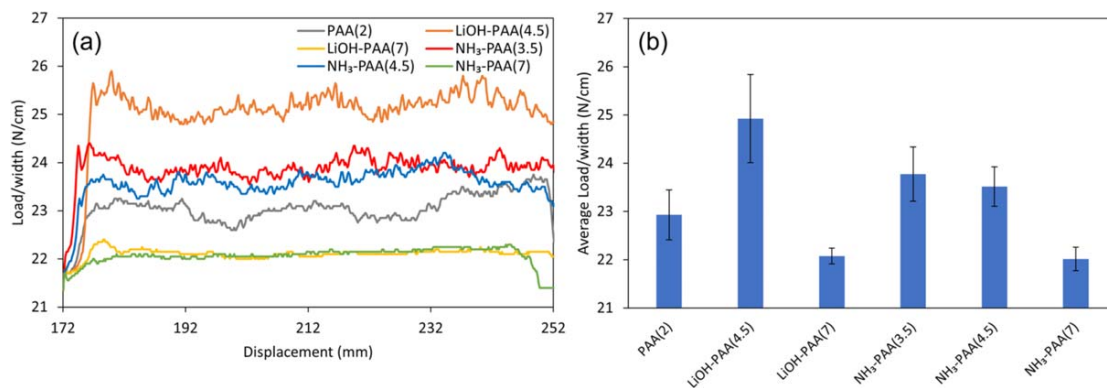


**Figure 5.** Results from peeling tests for silicon anodes fabricated using different binders: (a) load per unit width vs displacement and (b) corresponding averages.

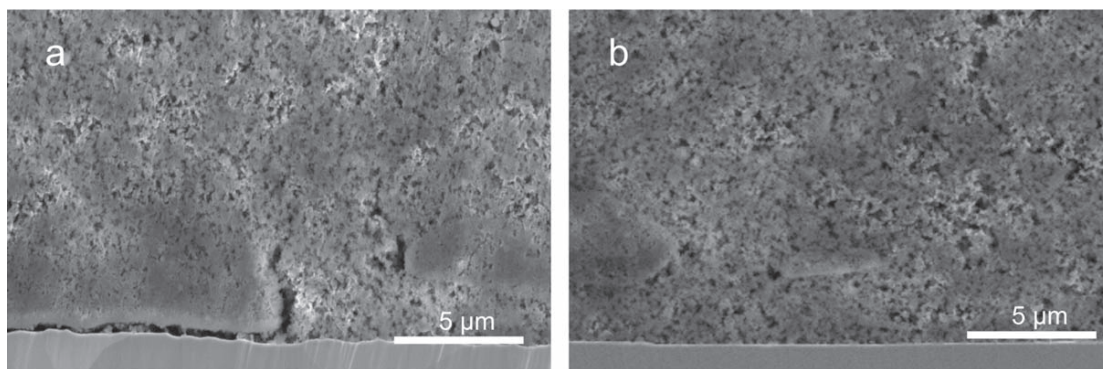


**Figure 6.** Representative cross-sectional images of electrode delamination of (a) NH<sub>3</sub>-PAA(7) anode vs well-connected (b) NH<sub>3</sub>-PAA(3.5) anode.

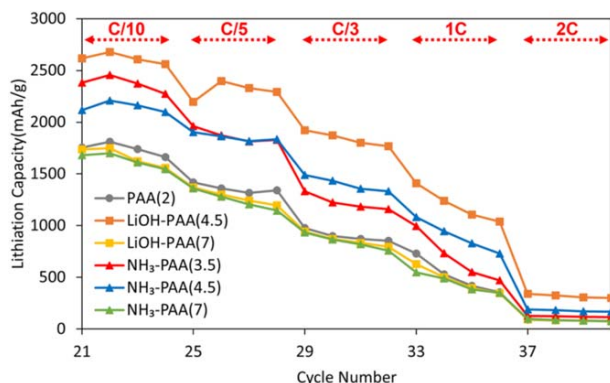


**Figure 7.** Average capacity of silicon half-cells for cycles 21–40 for varying C-rates and binders. The average standard error of points is 34 mAh g<sup>-1</sup> for two samples of each binder type.

materials; our results below show that some neutralization of acidic PAA does provide benefits consistent with the report by Hays et al.

**Mechanical integrity.**—Peeling test results showing mechanical integrity of PAA/Si electrode are included in Fig. 5. The figure shows a clear trend within the NH<sub>3</sub>-PAA series indicating that the average peeling force decreases moderately as the pH of the binder increases. For example, the average peeling force was 24 N cm<sup>-1</sup> for NH<sub>3</sub>-PAA(3.5) anode, while it was 22 N cm<sup>-1</sup> for NH<sub>3</sub>-PAA(7). Cross-sectional images of the electrodes (Fig. 6) demonstrate delamination of the electrode when using NH<sub>3</sub>-PAA(7) binder. Meanwhile, other electrode coatings in this study remained well-connected to the current collector. When comparing peeling results

between LiOH-PAA(4.5) and LiOH-PAA(7) electrodes, the same pH trend is observed.

It has been suggested in prior work that the raised pH value of PAA binder can be detrimental to the cohesion and adhesion in the electrode matrix. Namely, the absence of –COOH groups to build hydrogen bonds in neutralized PAA (e.g. LiOH-PAA(7) electrode) suggests weaker bonding between the binder and other materials or perhaps with itself. Dang et al. propose that the stretched chains of LiOH-PAA for pH around 4, which can anchor on the Si surface through hydrogen bonds, along with the –COOLi and –Si-OH ion-dipole interactions, can contribute to superior mechanical integrity,<sup>13</sup> which is consistent with our results. For our pristine PAA electrode, the low pH is detrimental to the uniform distribution of silicon, and this appears to also weaken electrode mechanical integrity.

Another view on the effect of lithiation on polymer interactions is given by Kwon et al.<sup>20</sup> They suggest that a lithiated polymer containing carboxylic acid groups led to stronger ion-dipole interactions and thereby increased cohesion between polymer chains and adhesion to Si particles. This polymer is distinct from PAA, but the results nevertheless suggest there can be subtle bonding effects and competition that could lead to an outcome different than observed here for neutralized PAA.

A further hypothesis to explain our observed variation in adhesion to the copper current collector with pH values is given by Xiong et al. They used both SEM-EDX and XPS quantitative measurements to show that reduced corrosion or etching of Cu at high pH values led to decreased electrode adhesion between copper and the electrode coating.<sup>21</sup> In addition, their scratch test that evaluated the quality of the adhesion of electrode on copper current collector further confirmed the worse adhesion between copper and electrode at high pH values. Our results are consistent with these, with the exception that our pristine PAA(2) electrode shows a

relatively low peeling force despite its low pH. As described above, this may be due to poor cohesion or integrity of the film itself.

**Cycling performance.**—Our results above suggest that (1) the introducing  $\text{Li}^+$  in the binder solution facilitates ion transport, and (2) increased pH can be beneficial for particle dispersion and mixing, though it can be detrimental to electrode mechanical integrity. To further investigate these findings on electrochemical performance, half-cell tests among these electrodes are compared in Fig. 7. When considering the effect of  $\text{Li}^+$ , LiOH-PAA(4.5) half-cell shows an average capacity  $500\sim 800\text{ mAh g}^{-1}$  higher than that of  $\text{NH}_3\text{-PAA}(4.5)$  throughout all charging rates. For instance, the LiOH-PAA(4.5) half-cell shows  $2600\text{ mAh g}^{-1}$  at C/5 and  $400\text{ mAh g}^{-1}$  at 2 C, while for the  $\text{NH}_3\text{-PAA}(4.5)$  half-cell, rate-dependent capacities are 1600 and  $100\text{ mAh g}^{-1}$ , respectively. The capacity increase due to LiOH further verifies that  $\text{Li}^+$  facilitates ion transport.

As for the effect of pH, while the  $\text{NH}_3\text{-PAA}(3.5)$  half-cell initially shows a higher electrochemical performance than that of  $\text{NH}_3\text{-PAA}(4.5)$  due to better particle adhesion/cohesion, the lower pH detrimental to the particle dispersion appears to cause lower capacity at higher C-rates. In addition, the cycling capacity shows the same trend as observed in peeling test where  $\text{LiOH-PAA}(4.5) > \text{NH}_3\text{-PAA}(3.5/4.5) > \text{PAA}(2) > \text{NH}_3\text{-PAA}(7)$ , LiOH-PAA(7). This implies that electrode adhesion has a higher impact on cell electrochemical performance than slurry viscosity does.

### Conclusions

Previously the effect of  $\text{Li}^+$  and pH from the introduction of lithium hydroxide into PAA binder was not well understood. In this study, we separate these two factors. CV and EIS tests demonstrate that the extra  $\text{Li}^+$  in the binder facilitates ion transport. As for the increased pH value, while it benefits the particle dispersion and slurry mixing, the anode mechanical integrity can be degraded. A cell composed of LiOH-PAA(4.5) not only has the advantage of  $\text{Li}^+$  enhancing ion transport, but also the moderate pH favorable to both hydrogen bonding and ion-dipole interaction with Si, all of which contribute to its improved performance when compared to other tested cells. It is true that prior work showed some disparity in performance advantage between PAA and LiOH-PAA. We cannot be sure of the exact causes; however, such differences could originate from material choices such as active material size, binder molecular weight, and electrolyte, and from manufacturing steps such as mixing and drying. If binder adhesion to the current collector is indicative of eventual cycling performance, as suggested in this

work, then this could be used as a diagnostic tool for evaluating future binders for silicon anodes.

### Acknowledgments

This work was partially supported by the U.S. Department of Energy Office of Science under contract DE-SC0021893. We would like to acknowledge the BYU Electron Microscopy Facility for providing access to the equipment and expertise that allowed this project to be performed.

### ORCID

Fei Sun  <https://orcid.org/0009-0009-8111-0183>

### References

1. S. Li, Y.-M. Liu, Y.-C. Zhang, Y. Song, G.-K. Wang, Y.-X. Liu, Z.-G. Wu, B.-H. Zhong, Y.-J. Zhong, and X.-D. Guo, *J. Power Sources*, **485**, 229331 (2021).
2. P. Li, H. Kim, S.-T. Myung, and Y.-K. Sun, *Energy Storage Mater.*, **35**, 550 (2021).
3. X. Zuo, J. Zhu, P. Müller-Buschbaum, and Y.-J. Cheng, *Nano Energy*, **31**, 113 (2017).
4. A. Franco Gonzalez, N.-H. Yang, and R.-S. Liu, *The Journal of Physical Chemistry C*, **121**, 27775 (2017).
5. L. Sun, Y. Liu, R. Shao, J. Wu, R. Jiang, and Z. Jin, *Energy Storage Materials*, **46**, 482 (2022).
6. C. Zhao, T. Wada, V. De Andrade, D. Gürsoy, H. Kato, and Y.-K. Chen-Wiegart, *Nano energy*, **52**, 381 (2018).
7. S. L. Mitchell and M. Ortiz, *J. Power Sources*, **326**, 242 (2016).
8. W. Huang, W. Wang, Y. Wang, Q. Qu, C. Jin, and H. Zheng, *J. Mater. Chem. A*, **9**, 1541 (2021).
9. P. Parikh, M. Sina, A. Banerjee, X. Wang, M. S. D'Souza, J.-M. Doux, E. A. Wu, O. Y. Trieu, Y. Gong, and Q. Zhou, *Chem. Mater.*, **31**, 2535 (2019).
10. Y. Wang, H. Xu, X. Chen, H. Jin, and J. Wang, *Energy Storage Mater.*, **38**, 121 (2021).
11. M. Ling, H. Zhao, X. Xiaoc, F. Shi, M. Wu, J. Qiu, S. Li, X. Song, G. Liu, and S. Zhang, *J. Mater. Chem. A*, **3**, 2036 (2015).
12. B. Hu, S. Jiang, I. A. Shkrob, J. Zhang, S. E. Trask, B. J. Polzin, A. Jansen, W. Chen, C. Liao, and Z. Zhang, *J. Power Sources*, **416**, 125 (2019).
13. D. Dang, Y. Wang, M. Wang, J. Hu, C. Ban, and Y.-T. Cheng, *ACS Appl. Energy Mater.*, **3**, 10940 (2020).
14. A. Michaels and O. Morelos, *Industrial & Engineering Chemistry*, **47**, 1801 (1955).
15. J. E. Vogel, J. G. Sederholm, E. M. Shumway, G. J. Abello, S. E. Trask, D. R. Wheeler, and B. A. Mazzeo, *J. Electrochem. Soc.*, **169**, 080508 (2022).
16. G. A. Luduena, T. D. Kühne, and D. Sebastiani, *Chem. Mater.*, **23**, 1424 (2011).
17. N. P. Pieczonka, V. Borgel, B. Ziv, N. Leifer, V. Dargel, D. Aurbach, J. H. Kim, Z. Liu, X. Huang, and S. A. Krachkovskiy, *Adv. Energy Mater.*, **5**, 1501008 (2015).
18. Z. Shi, S. Jiang, L. A. Robertson, Y. Zhao, E. Sarnello, T. Li, W. Chen, Z. Zhang, and L. Zhang, *ACS Appl. Mater. Interfaces*, **12**, 57932 (2020).
19. K. A. Hays, B. Armstrong, and G. M. Veith, *ChemElectroChem*, **7**, 3790 (2020).
20. T. w. Kwon, Y. K. Jeong, I. Lee, T. S. Kim, J. W. Choi, and A. Coskun, *Adv. Mater.*, **26**, 7979 (2014).
21. J. Xiong, N. Dupré, D. Mazouzi, D. Guyomard, L. Roué, and B. Lestriez, *ACS Appl. Mater. Interfaces*, **13**, 28304 (2021).